Globally Optimal Symbolic Hand-Eye Calibration

Jin Wu, *Member, IEEE*, Ming Liu, *Senior Member, IEEE*, Yilong Zhu, Zuhao Zou, Ming-Zhe Dai, Chengxi Zhang, *Member, IEEE*, Yi Jiang, *Member, IEEE* and Chong Li

***Abstract*— Hand-eye calibration (HEC) is a kernel technique guaranteeing precision industrial visual servoing and robotic grasping. Extensive studies have been conducted to various closed-form and iterative solutions to HEC problems using different pose parameterizations. However, these approaches are either sensitive to input noise or time-consuming for implementation. This paper provides a new perspective on a deterministic solution to two major branches of HEC problems of forms AX = XB and AX = YB. We use symbolic methods to derive a globally optimal solution. Different from representatives based on optimization, this method is not only the most accurate against others but also with repeatability of 100%. Experiments via industrial robotic manipulator verify the superiority of the proposed algorithm.**

***Index Terms*— Hand-eye calibration, robotic perception, symbolic computation, robotic manipulator, global solution.**

I. Introduction

A. Motivations

VARIOUS industrial tasks require accurate grasping of cargos and objects using robotic manipulators. The visual measurements provide such a technique for perception but the frame of the mounted camera may usually not be united with that of the manipulator's flange [1], [2]. Hand-eye calibration (HEC) aims to solve this problem by computing the extrinsic parameter between the camera and the robotic end-effector [3]. It is also noted that hand-eye relationship is also useful for attitude determination with respect to an ellipsoidal object like astroid [4], [5]. Depicted in Fig. 1, the classical HEC problem takes the form of $\boldsymbol{AX} = \boldsymbol{XB}$ in black, where $\boldsymbol{A}$, $\boldsymbol{B}$ are relative transformations of the camera (red part) and the end-effector (blue part), respectively. An improvement of the $\boldsymbol{AX} = \boldsymbol{XB}$ HEC considers the eye-hand transformation $\boldsymbol{X}$ and the robot-world transformation $\boldsymbol{Y}$ simultaneously so that the equation $\boldsymbol{AX} = \boldsymbol{YB}$ is established. Note that the matrices $\boldsymbol{A}, \boldsymbol{B}$ have the different meaning with that in HEC problem of $\boldsymbol{AX} = \boldsymbol{XB}$, i.e. $\boldsymbol{A}$ denotes the camera-world transformation and $\boldsymbol{B}$ is the pose of end-effector in the robot frame. In the following contents, we do not use additional colors to distinguish the two HEC problems. Rather, they are considered more in a mathematical manner.

In this paper, a global semi-symbolic solution to HEC problems has been reported. This work has the purpose of solving some longstanding challenges in accurate and efficient HEC computation, i.e.:

1) Although many closed-form solutions have been developed, they are sensitive to input noise and outliers. This is because hand-eye calibration is essentially non-convex thus any closed-form solution will only be an approximate answer.
2) The $\boldsymbol{AX} = \boldsymbol{XB}$ and $\boldsymbol{AX} = \boldsymbol{YB}$ problems are both nonlinear so optimizers may sink into local minima.
3) As many searchings are trivial, finding the globally optimal solution is always computationally inefficient.

The above three challenges are not well solved in previous literatures and still preserve large potential to benefit the community. In fact, online finding a globally optimal solution efficiently is important for industrial robots, as for some cases the eye-hand extrinsic parameters may vary while working. Also, the accuracy of obtained HEC results will be significantly influential to further tasks including grasping and uncertainty evaluation.

B. Related Work

The background of the studied problems are presented in the 3-dimensional (3-D) world. Thus the homogeneous transformations are parameterized via the 3-D special Euclidean group $SE(3)$, which is formed by homogeneous combination of 3-D rotation $\boldsymbol{R}$ and translation $\boldsymbol{t}$ such that a homogeneous transformation $\boldsymbol{T}$ is constructed by the SE operator

$$\boldsymbol{T} = \begin{pmatrix} \boldsymbol{R} & \boldsymbol{t} \\ \boldsymbol{0} & 1 \end{pmatrix} = SE(\boldsymbol{R}, \boldsymbol{t}) \in SE(3). \tag{1}$$

HEC problems are nonlinear mainly because the rotation matrix $\boldsymbol{R}$ has nonlinear constraints $\boldsymbol{R}^\top \boldsymbol{R} = \boldsymbol{I}, \det(\boldsymbol{R}) = +1$ i.e. $\boldsymbol{R}$ being an element of the special orthogonal group $SO(3)$. Therefore, since 1980s, many efforts have been paid to give closed-form solutions based on diverse pose parameterizations, including rotation vector [6], quaternion [7], dual quaternion

Manuscript received 22 May, 2020; revised 27 July, 2020; accepted 22 August, 2020. Date of publication X X, 20XX; date of current version X X, 20XX. Recommended by Editor H. Qiao. This research was supported by Shenzhen Science, Technology and Innovation Comission (SZSTI) JCYJ20160401100022706, in part by General Research Fund of Research Grants Council Hong Kong, 11210017, in part by Early Career Scheme Project of Research Grants Council Hong Kong, 21202816. (*Corresponding author: Ming Liu*).

J. Wu, M. Liu, Y. Zhu and Z. Zou are with Department of Electronic and Computer Engineering, Hong Kong University of Science and Technology, Hong Kong, China. (e-mail: eelium@ust.hk).

M. Dai is with the School of Aeronautics and Astronautics, Central South University, Changsha 410083, China (e-mail: mingzhe_dai@csu.edu.cn)

C. Zhang is with School of Electronic and Information Engineering, Harbin Institute of Technology, Harbin, China. (e-mail: dongfangxy@163.com)

Y. Jiang is with the State Key Laboratory of Synthetical Automation for Process Industries and International Joint Research Laboratory of Integrated Automation, Northeastern University, Shenyang, China. (e-mail: JY369356904@163.com)

C. Li is with Department of Automation & Measurement, Ocean University of China, Qingdao, China. (e-mail: czl0047@auburn.edu)

Digital Object Identifier 10.1109/TMECH.20XX.XXXX

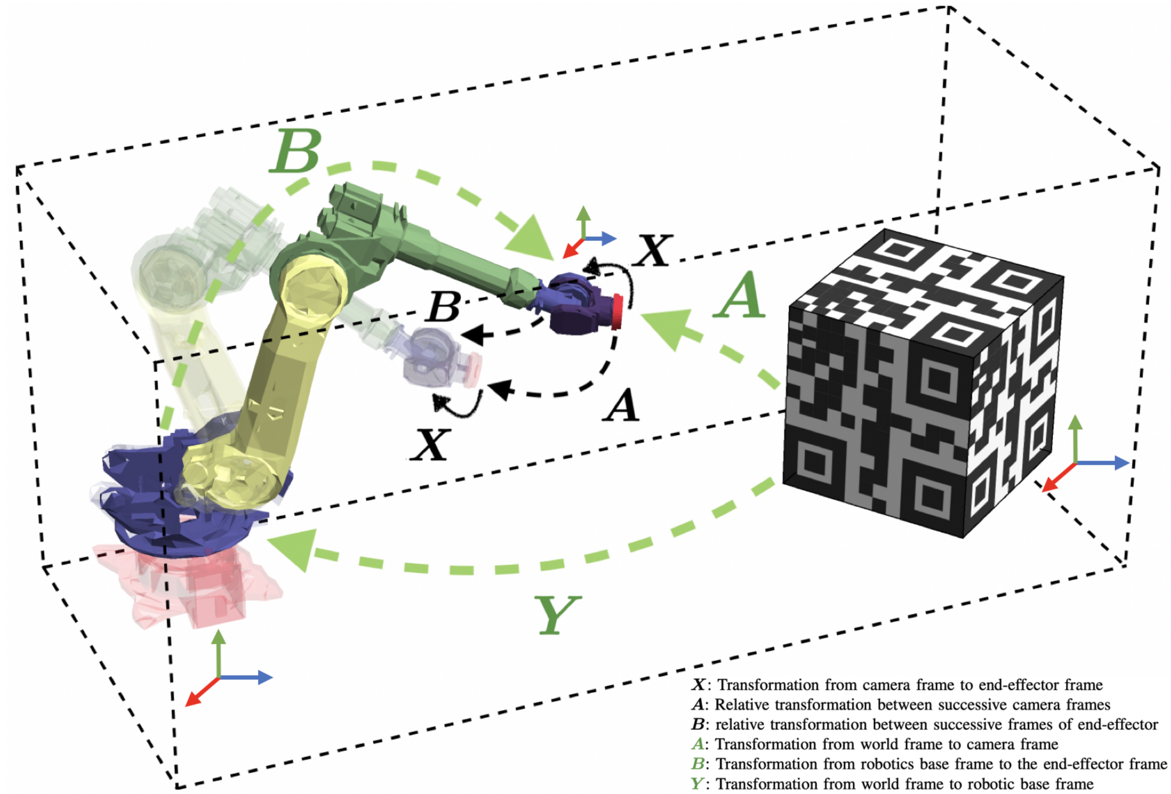

Fig. 1. The hand-eye and robot-world relationships $\boldsymbol{AX} = \boldsymbol{XB}$ and $\boldsymbol{AX} = \boldsymbol{YB}$. The standard object is a box of quick response (QR) codes, which denotes the world frame.

[8], screw parameters [9] and etc. [10]. Analytical results also show some strong connections to point cloud matching like iterative closest point (ICP) [11], [12]. Furthermore, as the forms of $\boldsymbol{AX} = \boldsymbol{XB}$ and $\boldsymbol{AX} = \boldsymbol{YB}$ decide that rotation and translation parts of unknowns $\boldsymbol{X}, \boldsymbol{Y}$ are coupled together, solving $\boldsymbol{R}$ and $\boldsymbol{t}$ separately does achieve the global optimum [13]. Therefore, an accurate solution can hardly be obtained using only closed-form results. Instead, the starting from a rough analytical solution, iterative solution tries to find out a refined estimate [14], [15]. However, as a proper initial guess may not exist in analytical results, such iterative solution would also tend to fail in datasets with numerous outliers. Therefore, recently researchers have tend to find globally optimal solution to HEC problems without the knowledge of any initial guess. Heller et al. solve the problem based on a Branch-and-Bound (BnB) strategy for outlier rejection and rotation searching [16]. For an $\boldsymbol{AX} = \boldsymbol{YB}$ case as pose estimation of a quadrotor, Ha et al. developed uniform sampling on $SO(3)$ for global optimization [17]. Likewise, for globally optimal ICP solvers, BnB and uniform rotation sampling are also vital and practical [18], [19]. Actually, there are many other calibration tasks that can be considered in a hand-eye manner, e.g. the camera-laser calibration [20], camera-magnetometer calibration [21], binocular extrinsic calibration [22] and etc. These multiple data sources also bring different data structures and will lead to various special cases in hand-eye calibration, which makes globally optimal solving the problem more challenging in engineering. However, since there are infinite possible uniform rotation samplings as initial guesses, it is not likely to compute a globally optimal result within short time. And for all these global algorithms, there is no guarantee that for a certain set we can always find the globally optimal solution. That is to say, we need to answer a kernel question: how many local minima are there in hand-eye problems? This is actually the complete solution classification, which is the main problem that we need to solve in this paper.

C. Contribution

Guided by existing research results of HEC problems, contributions of this paper are briefly listed as follows

1) The HEC optimization frameworks have been revisited. It is shown that the coupling between the rotation and translation can be fixed, generating a new system containing unknowns of rotation only.
2) To find the globally optimal solution, the newly derived system is solved in a symbolic manner. We cast the problem for the first time into a solvable series of high-order polynomials, which can be easily simplified and solved via mainstream computer algebra systems.
3) The global optimum can be found be sorting all the loss function values while the repeatability of the method is 100%. We give exact numbers of possible local minima by algebraic theorems.

D. Outline

The remainder of this paper is structured as follows: Section II presents our new theory and symbolic solution to the HEC problems. Synthetic and experimental results have been evaluated in Section III show efficiency of the proposed method compared with representatives. While we draw concluding remarks in Section IV, some future expectations are illustrated as well.

II. Proposed Globally Optimal Solution

A. Notations

The n-dimensional real Euclidean space is represented by $\mathbb{R}^n$ containing all real n-dimensional vectors. The Euclidean norm of a squared matrix $\boldsymbol{X}$ is $\|\boldsymbol{X}\| = \sqrt{\mathrm{tr}\left(\boldsymbol{X}^\top \boldsymbol{X}\right)}$ in which the symbol $\mathrm{tr}(\cdot)$ denotes the matrix trace. For a given arbitrary matrix $\boldsymbol{X}$, $\boldsymbol{X}^\dagger$ is called its Moore-Penrose generalized inverse. Given a 3-D vector $\boldsymbol{x} = (x_1, x_2, x_3)^\top$, its associated skew-symmetric matrix is defined in

$$\boldsymbol{x}_\times = \begin{pmatrix} 0 & -x_3 & x_2 \\ * & 0 & -x_1 \\ * & * & 0 \end{pmatrix} \tag{2}$$

which belongs to the $\mathfrak{so}(3)$ group and $*$ denotes the skew symmetry. Any rotation $\boldsymbol{R}$ on the $SO(3)$ has its corresponding logarithm i.e. $\boldsymbol{x}_\times = \log(\boldsymbol{R})$ so that $\exp(\boldsymbol{x}_\times) = \boldsymbol{I} + \boldsymbol{x}_\times + \boldsymbol{x}_\times^2/2! + \cdots$. The inverse map i.e. the wedge operation $\wedge$ from the 3×3 skew-symmetric matrix to the 3-D vector is denoted as $\boldsymbol{x}_\times^\wedge = \boldsymbol{x}$.

B. Hand-Eye Optimization

For measurement noise adjustment, HEC problems are processed via optimizations, such that

$$\mathop{\arg\min}_{\boldsymbol{X},\boldsymbol{Y} \in SE(3)} \mathcal{L} = \sum_{i=1}^{N} \|\boldsymbol{A}_i \boldsymbol{X} - \boldsymbol{Y} \boldsymbol{B}_i\|^2 \tag{3}$$

in which $\boldsymbol{A}_i$ and $\boldsymbol{B}_i$ are measurements for the i-th time instant and $\boldsymbol{X}, \boldsymbol{Y}$ are to be figured out which distribute on $SE(3)$. N denotes the number of measurements that we gathered historically. When $\boldsymbol{X} = \boldsymbol{Y}$, the result problem is of the form $\boldsymbol{AX} = \boldsymbol{XB}$ that only considers the eye-hand relationship. Note that $\boldsymbol{X}$ and $\boldsymbol{Y}$ here are considered as constants according to fixed installation of camera and robot base. The target loss function can be expanded to

$$\mathcal{L} = \sum_{i=1}^{N} \mathrm{tr}\left(\begin{matrix} \boldsymbol{X}^\top \boldsymbol{A}_i^\top \boldsymbol{A}_i^\top \boldsymbol{X}^\top - \boldsymbol{B}_i^\top \boldsymbol{Y}^\top \boldsymbol{A}_i \boldsymbol{X} \\ -\boldsymbol{X}^\top \boldsymbol{A}_i^\top \boldsymbol{Y} \boldsymbol{B}_i + \boldsymbol{B}_i \boldsymbol{Y}^\top \boldsymbol{Y} \boldsymbol{B}_i^\top \end{matrix}\right). \tag{4}$$

For clarification, $\mathcal{L}_1$ and $\mathcal{L}_2$ are invoked for representation of target loss functions of problems $\boldsymbol{AX} = \boldsymbol{XB}$ and $\boldsymbol{AX} = \boldsymbol{YB}$, respectively. Actually, these two problems are highly related in mathematics. If we transform both sides of the equation $\boldsymbol{AX} = \boldsymbol{XB}$ using a known transformation $\boldsymbol{Z}$, the new formulation is $\boldsymbol{ZAXZ} = \boldsymbol{ZXBZ}$. By letting $\tilde{\boldsymbol{A}} = \boldsymbol{ZA}, \tilde{\boldsymbol{X}} = \boldsymbol{XZ}, \tilde{\boldsymbol{Y}} = \boldsymbol{ZX}, \tilde{\boldsymbol{B}} = \boldsymbol{BZ}$, it is able for us to reconstruct the problem as $\tilde{\boldsymbol{A}}\tilde{\boldsymbol{X}} = \tilde{\boldsymbol{Y}}\tilde{\boldsymbol{B}}$. A potential effect of introducing $\boldsymbol{Y}$ is that using more accurate $\boldsymbol{B}$ matrix, the $\boldsymbol{X}$ matrix in problem $\boldsymbol{AX} = \boldsymbol{YB}$ can be estimated more precisely. To solve these optimization problems, Gwak et al. and Ha et al. both studied the gradient and Newton minimization of (4) using Lie algebra, where the approximate closed forms of the Jacobians are given. Quaternions are also considered historically by Horaud et al. [14], [15], which has been improved recently by Heller et al. who introduced the linear matrix inequality (LMI) relaxation to solve the target optimization [23]. However, all these classical methods are derivative-based and tend to suffer from local minima, leading to an unfortunate fact that finding a globally optimal solution without initial guess may sometimes be trivial.

Let us rethink about the HEC problem $\boldsymbol{AX} = \boldsymbol{YB}$. Many algorithms solve the problem via Lie algebra of the rotation. However, according to infinity terms of Lie exponential, the Jacobian matrix can only be approximated. Besides, quaternions, dual quaternions, rotation matrices all have their own nonlinear constraints and will bring burden for further optimization. Therefore, it is required to use another rotation parameterization that owns deterministic formula of Jacobian without any constraint. Historically, this may be achieved by the Cayley transformation such that one rotation can be written in the form of

$$\boldsymbol{R} = (\boldsymbol{I} + \boldsymbol{G})^{-1} (\boldsymbol{I} - \boldsymbol{G}) \tag{5}$$

where $\boldsymbol{G}$ denotes a skew-symmetric matrix such that $\boldsymbol{g}_\times = \boldsymbol{G}$. Alternatively, $\boldsymbol{R}$ can also be written in terms of

$$\boldsymbol{R} = (\boldsymbol{I} - \boldsymbol{G}) (\boldsymbol{I} + \boldsymbol{G})^{-1} \tag{6}$$

The problem $\boldsymbol{AX} = \boldsymbol{YB}$ can be parameterized independently via

$$\boldsymbol{R_A R_X} = \boldsymbol{R_Y R_B} \tag{7}$$

$$\boldsymbol{R_A t_X} + \boldsymbol{t_A} = \boldsymbol{R_Y t_B} + \boldsymbol{t_Y} \tag{8}$$

where $\boldsymbol{R_X}, \boldsymbol{t_X}$ and $\boldsymbol{R_Y}, \boldsymbol{t_Y}$ denote the rotation and translation parts of poses $\boldsymbol{X}$ and $\boldsymbol{Y}$, respectively. Let $\boldsymbol{R_X} = (\boldsymbol{I} + \boldsymbol{G_X})(\boldsymbol{I} - \boldsymbol{G_X})^{-1}$, $\boldsymbol{R_Y} = (\boldsymbol{I} + \boldsymbol{G_Y})^{-1}(\boldsymbol{I} - \boldsymbol{G_Y})$ and $\boldsymbol{g}_{\boldsymbol{X},\times} = \boldsymbol{G_X}$, $\boldsymbol{g}_{\boldsymbol{Y},\times} = \boldsymbol{G_Y}$. We are able to transform $\boldsymbol{R_A R_X} = \boldsymbol{R_Y R_B}$ as

$$(\boldsymbol{I} + \boldsymbol{G_Y}) \boldsymbol{R_A} (\boldsymbol{I} + \boldsymbol{G_X}) = (\boldsymbol{I} - \boldsymbol{G_Y}) \boldsymbol{R_B} (\boldsymbol{I} - \boldsymbol{G_X}) \tag{9}$$

which can be arranged as

$$\boldsymbol{C} + \boldsymbol{G_Y D} + \boldsymbol{D G_X} + \boldsymbol{G_Y C G_X} = \boldsymbol{0} \tag{10}$$

where $\boldsymbol{C} = \boldsymbol{R_A} - \boldsymbol{R_B}$ and $\boldsymbol{D} = \boldsymbol{R_A} + \boldsymbol{R_B}$. Likewise, the translation part can be evaluated as

$$(\boldsymbol{I} + \boldsymbol{G_Y})(\boldsymbol{R_A t_X} + \boldsymbol{t_A} - \boldsymbol{t_Y}) - (\boldsymbol{I} - \boldsymbol{G_Y}) \boldsymbol{t_B} = \boldsymbol{0}. \tag{11}$$

By letting $\boldsymbol{E}_i = \boldsymbol{C}_i + \boldsymbol{g}_{\boldsymbol{Y},\times} \boldsymbol{D}_i + \boldsymbol{D}_i \boldsymbol{g}_{\boldsymbol{X},\times} + \boldsymbol{g}_{\boldsymbol{Y},\times} \boldsymbol{C}_i \boldsymbol{g}_{\boldsymbol{X},\times}$ and $\boldsymbol{v}_i = (\boldsymbol{I} + \boldsymbol{g}_{\boldsymbol{Y},\times})(\boldsymbol{R}_{\boldsymbol{A},i} \boldsymbol{t_X} + \boldsymbol{t}_{\boldsymbol{A},i} - \boldsymbol{t_Y}) - (\boldsymbol{I} - \boldsymbol{g}_{\boldsymbol{Y},\times}) \boldsymbol{t}_{\boldsymbol{B},i}$, it is able to reformulate (3) as

$$\mathop{\arg\min}_{\boldsymbol{g_X},\boldsymbol{g_Y},\boldsymbol{t_X},\boldsymbol{t_Y} \in \mathbb{R}^3} \tilde{\mathcal{L}} = \sum_{i=1}^{N} \mathrm{tr}\left(\boldsymbol{E}_i^\top \boldsymbol{E}_i\right) + \boldsymbol{v}_i^\top \boldsymbol{v}_i \tag{12}$$

which is an unconstrained optimization for $\boldsymbol{g_X}, \boldsymbol{g_Y}, \boldsymbol{t_X}, \boldsymbol{t_Y}$. When we deal with the problem $\boldsymbol{AX} = \boldsymbol{XB}$, we have $\boldsymbol{g_X} = -\boldsymbol{g_Y}, \boldsymbol{t_X} = \boldsymbol{t_Y}$ which can be easily computed in a similar manner. To distinguish the target functions of $\boldsymbol{AX} = \boldsymbol{XB}$ and $\boldsymbol{AX} = \boldsymbol{YB}$, we use $\tilde{\mathcal{L}}_1$ and $\tilde{\mathcal{L}}_2$ respectively.

C. Algebraic Polynomials and Roots

Equation (12) presents an optimization with least number of variables. Using $\boldsymbol{x} = \left(\boldsymbol{g}_{\boldsymbol{X}}^\top, \boldsymbol{t}_{\boldsymbol{X}}^\top\right)^\top$ and $\boldsymbol{y} = \left(\boldsymbol{g}_{\boldsymbol{Y}}^\top, \boldsymbol{t}_{\boldsymbol{Y}}^\top\right)^\top$ as state vectors of unknown variables $\boldsymbol{X}$ and $\boldsymbol{Y}$ respectively, it is clear that the gradient searching is achieved by

$$\boldsymbol{x}_k = \boldsymbol{x}_{k-1} - \mu \nabla_{\boldsymbol{x}} \tilde{\mathcal{L}}_1(\boldsymbol{x}_{k-1}) \tag{13}$$

$$\boldsymbol{z}_k = \boldsymbol{z}_{k-1} - \mu \nabla_{\boldsymbol{z}} \tilde{\mathcal{L}}_2(\boldsymbol{z}_{k-1}) \tag{14}$$

in which $\boldsymbol{z} = \left(\boldsymbol{x}^\top, \boldsymbol{y}^\top\right)^\top$ denotes the unified vector of $\boldsymbol{x}$ and $\boldsymbol{y}$, $k = 1, 2, \cdots$ is the optimization updating index and $\mu > 0$ stands for a step length. For HEC problems, all feasible local minima must satisfy

$$\lim_{k \to +\infty} \nabla_{\boldsymbol{x}} \tilde{\mathcal{L}}_1(\boldsymbol{x}_k) = \boldsymbol{0}, \quad \lim_{k \to +\infty} \nabla_{\boldsymbol{z}} \tilde{\mathcal{L}}_2(\boldsymbol{z}_k) = \boldsymbol{0}. \tag{15}$$

Here one needs to note that the zero sets of $\nabla_{\boldsymbol{x}} \tilde{\mathcal{L}}_1(\boldsymbol{x}_k) = \boldsymbol{0}, \nabla_{\boldsymbol{z}} \tilde{\mathcal{L}}_2(\boldsymbol{z}_k) = \boldsymbol{0}$ actually form all possible local minima. Therefore, solving the two systems algebraically gives complete sets of local minima which provides the global minimum that corresponds to the least value of loss functions.

Since $\boldsymbol{x}, \boldsymbol{y} \in \mathbb{R}^6$, $\nabla_{\boldsymbol{x}} \tilde{\mathcal{L}}_1(\boldsymbol{x}_k) = \boldsymbol{0}, \nabla_{\boldsymbol{z}} \tilde{\mathcal{L}}_2(\boldsymbol{z}_k) = \boldsymbol{0}$ have the sizes of 6×1 and 12×1 respectively. Equation (12) contains a strong multiplicative coupling between rotation and translation so let us first investigate the structure of the two system. Via symbolic computation, one can easily verify that $\nabla_{\boldsymbol{x}} \tilde{\mathcal{L}}_1(\boldsymbol{x}) = \boldsymbol{0}$ can be written in the following form

$$\begin{cases} f_1\left(\boldsymbol{g}_{\boldsymbol{X}}^3, \boldsymbol{g}_{\boldsymbol{X}}^2 \boldsymbol{t}_{\boldsymbol{X}}, \boldsymbol{g}_{\boldsymbol{X}} \boldsymbol{t}_{\boldsymbol{X}}^2, \boldsymbol{g}_{\boldsymbol{X}}, \boldsymbol{t}_{\boldsymbol{X}}\right) = \boldsymbol{0} \in \mathbb{R}^3 \\ f_2\left(\boldsymbol{g}_{\boldsymbol{X}}^2 \boldsymbol{t}_{\boldsymbol{X}}, \boldsymbol{g}_{\boldsymbol{X}}^2, \boldsymbol{g}_{\boldsymbol{X}}, \boldsymbol{t}_{\boldsymbol{X}}\right) = \boldsymbol{0} \in \mathbb{R}^3 \end{cases} \tag{16}$$

where $\boldsymbol{g}_{\boldsymbol{X}}^i$ denotes the combinatorial terms of $\boldsymbol{g}_{\boldsymbol{X}}$ of order i and $\boldsymbol{q}_{\boldsymbol{X}}^i \boldsymbol{t}_{\boldsymbol{X}}^j$ stands for all the products between elements of $\boldsymbol{g}_{\boldsymbol{X}}^i$ and $\boldsymbol{t}_{\boldsymbol{X}}^j$; f represents polynomial systems. Equation (16) is a typical polynomial system of $\boldsymbol{g}_{\boldsymbol{X}}$ and $\boldsymbol{t}_{\boldsymbol{X}}$ whose algebraic solutions are hard to be found out. From f_2 we can compute $\boldsymbol{t}_X$ in terms of $\boldsymbol{g}_{\boldsymbol{X}}$ which is presented in an inverse of a matrix whose components are $\boldsymbol{g}_{\boldsymbol{X}}^2$ and $\boldsymbol{g}_{\boldsymbol{X}}$. Therefore $\boldsymbol{t}_{\boldsymbol{X}}$ are in the form with numerator of order up to 4 and denominator of order up to 6. Thus, replacing $\boldsymbol{t}_{\boldsymbol{X}}$ in (16) thus gives a high-order system of $\boldsymbol{g}_{\boldsymbol{X}}$

$$f_3\left(\boldsymbol{g}_{\boldsymbol{X}}^{15}, \boldsymbol{g}_{\boldsymbol{X}}^{14}, \boldsymbol{g}_{\boldsymbol{X}}^{13}, \boldsymbol{g}_{\boldsymbol{X}}^{12}, \boldsymbol{g}_{\boldsymbol{X}}^{10}, \boldsymbol{g}_{\boldsymbol{X}}^{9}, \boldsymbol{g}_{\boldsymbol{X}}^{8}, \cdots\right) = \boldsymbol{0} \in \mathbb{R}^3 \tag{17}$$

The monomials with highest order of 15 has been obtained by eliminating the denominator of $\boldsymbol{t}_{\boldsymbol{X}}$ such that the term of highest order is $\boldsymbol{g}_{\boldsymbol{X}}^3$ and the order is computed by $3 + 6 \times 2 = 15$. Polynomial (17) has at most 243 unique solutions by Sturm's theorem and Bezout's theorem. These theorems have been extensively applied for root counting of polynomials. For instance, the renowned software Mathematica has a command of `RootIntervals` for exact root counting. The command `RootIntervals` has been implemented using Sturm's theorem in combination with Bezout's theorem for accurate root counting. For the problem $\boldsymbol{AX} = \boldsymbol{YB}$, we are able to obtain the following polynomials of $\nabla_{\boldsymbol{z}} \tilde{\mathcal{L}}_1(\boldsymbol{z}) = \boldsymbol{0}$

$$\begin{cases} f_4\left(\boldsymbol{g}_{\boldsymbol{X}} \boldsymbol{g}_{\boldsymbol{Y}}^2, \boldsymbol{g}_{\boldsymbol{X}} \boldsymbol{g}_{\boldsymbol{Y}}, \boldsymbol{g}_{\boldsymbol{Y}}^2, \boldsymbol{g}_{\boldsymbol{X}}, \boldsymbol{g}_{\boldsymbol{Y}}\right) = \boldsymbol{0} \in \mathbb{R}^3 \\ f_5\left(\boldsymbol{g}_{\boldsymbol{Y}}^2 \boldsymbol{t}_{\boldsymbol{X}}, \boldsymbol{g}_{\boldsymbol{Y}}^2 \boldsymbol{t}_{\boldsymbol{Y}}, \boldsymbol{g}_{\boldsymbol{Y}}^2, \boldsymbol{g}_{\boldsymbol{Y}}, \boldsymbol{t}_{\boldsymbol{X}}, \boldsymbol{t}_{\boldsymbol{Y}}\right) = \boldsymbol{0} \in \mathbb{R}^3 \\ f_6\begin{pmatrix} \boldsymbol{g}_{\boldsymbol{Y}} \boldsymbol{t}_{\boldsymbol{X}} \boldsymbol{t}_{\boldsymbol{Y}}, \boldsymbol{g}_{\boldsymbol{Y}} \boldsymbol{t}_{\boldsymbol{Y}}^2, \boldsymbol{g}_{\boldsymbol{Y}} \boldsymbol{t}_{\boldsymbol{X}}^2, \boldsymbol{g}_{\boldsymbol{X}}^2 \boldsymbol{g}_{\boldsymbol{Y}}, \boldsymbol{g}_{\boldsymbol{Y}} \boldsymbol{t}_{\boldsymbol{X}}, \\ \boldsymbol{g}_{\boldsymbol{Y}} \boldsymbol{t}_{\boldsymbol{Y}}, \boldsymbol{g}_{\boldsymbol{X}} \boldsymbol{g}_{\boldsymbol{Y}}, \boldsymbol{g}_{\boldsymbol{X}}^2, \boldsymbol{g}_{\boldsymbol{X}}, \boldsymbol{g}_{\boldsymbol{Y}}, \boldsymbol{t}_{\boldsymbol{X}}, \boldsymbol{t}_Y \end{pmatrix} = \boldsymbol{0} \in \mathbb{R}^3 \\ f_7\left(\boldsymbol{g}_{\boldsymbol{Y}}^2 \boldsymbol{t}_{\boldsymbol{X}}, \boldsymbol{g}_{\boldsymbol{Y}}^2 \boldsymbol{t}_{\boldsymbol{Y}}, \boldsymbol{g}_{\boldsymbol{Y}}^2, \boldsymbol{g}_{\boldsymbol{Y}}, \boldsymbol{t}_{\boldsymbol{X}}, \boldsymbol{t}_{\boldsymbol{Y}}\right) = \boldsymbol{0} \in \mathbb{R}^3 \end{cases} \tag{18}$$

which has at most 1080 unique solutions in theory. Note that the solution numbers are given to their largest extent simply because that in some cases the HEC problems degenerate. For instance, in some pure translation motions, the rotation may be unobservable leading to the fact that some degrees of freedom are lost. In those cases, some symbolic items may vanish which formulates some new systems with less complexity. Another condition may possibly occur is that in some cases, repeated roots will take place, due to which the number of unique solutions will also be deceased. The solution numbers are also affected by different N. When $N = 1$, the HEC problems are completely unsolvable, leading to multiple optimal solutions. When $N \geq 2$, the systems may be solvable but also depends on the structure of $\boldsymbol{A}$ and $\boldsymbol{B}$.

To give all possible solutions, automated reasoning methods are introduced for accurate and efficient solutions. We introduce the Wu's elimination for solving the algebraic systems (17) and (18). Wu's method was proposed by Wen-Tsun Wu in 1970s [24], [25], which was based on the mathematical mechanisms from classical mathematical literatures in ancient China. For instance the *The Nine Chapters on the Mathematical Art* and *Dayan Qiuyi Shu* are two representatives describing highly structured algebraic methods for elementary equation problems, which have large impact on later algorithms e.g. the RSA encryption algorithm developed in 1977 [26]. Wu extended the ancient approaches to a systematic theory for automated reasoning. As such, not only nonlinear algebraic equations can be solved, proofs of geometric problems can be completed by computers as well, which is called the mechanical theorem proving. Consider a general polynomial system

$$\begin{cases} \mathcal{I}_1(p_1, p_2, \cdots, p_k) = 0 \\ \mathcal{I}_2(p_1, p_2, \cdots, p_k) = 0 \\ \qquad \vdots \\ \mathcal{I}_m(p_1, p_2, \cdots, p_k) = 0 \end{cases} \tag{19}$$

where k unknowns can be categorized into a vector $\boldsymbol{p} = (p_1, p_2, \cdots, p_k)^\top$ and $\mathcal{I}_1, \cdots, \mathcal{I}_m$ stand for polynomial system of m equations. We call $\varnothing_{\boldsymbol{p}}^{\mathcal{I}}$ the set of roots such that the polynomial set $\mathcal{I} = (\mathcal{I}_1, \mathcal{I}_2, \cdots, \mathcal{I}_m) = 0$, which is also called an ideal in abstract algebra. We call the following polynomial system a triangularized one

$$\begin{cases} \mathcal{I}_1(p_1) = 0 \\ \mathcal{I}_2(p_1, p_2) = 0 \\ \quad \vdots \\ \mathcal{I}_m(p_1, p_2, \cdots, p_k) = 0. \end{cases} \tag{20}$$

Moreover, a triangularized one is the characteristic set if it satisfies some conditions. To obtain the characteristic set of $\mathcal{I}$, one needs to refer to symbolic manipulations, eliminations and substitutions. Using Groebner bases can also achieve such simplification. However, Groebner-basis method requires to determine complete set of monomials involved. When encountering degenerate cases, previously generated Groebner bases become ill-posed and require re-computation which is very slow even for modern computers. Wu's method focuses on finding deterministic form of the characteristic set via computer algebra with a certain series of operations. It will point out whether $\mathcal{I}$ is solvable or not. Then, if $\mathcal{I} = 0$ is solvable, the set of roots is constructed using Wu's theorem, such that

$$\varnothing_{\boldsymbol{p}}^{\mathcal{I}} = \varnothing_{\boldsymbol{p}}^{\mathcal{S}} + \sum_i \varnothing_{\boldsymbol{p}}^{\mathcal{B}_i} \tag{21}$$

in which $\mathcal{S}$ denotes the remainder of the polynomial devision of the polynomial set $\mathcal{C}$ using a guessed solution (may come from iterative methods); $\mathcal{B}_i$ denotes the augmented polynomial set using guessed solution for i-th polynomial. Wu's method is computer-friendly and can be implemented using diverses advanced programming languages e.g. MATLAB, Mathematica, Maple, Symbolic C++ and etc. We need to note that, for many mainstream symbolic softwares, floating-point numbers are not supported for symbolic manipulations. Therefore, when implementing the related algorithms, the stored floating numbers should be simultaneously scaled to a large degree so that they can be converted to integers without loss of precision.

III. Experimental Results

We implement the symbolic computation using combined approach of Symbolic C++ and MATLAB-C++ interface. All the experiments are conducted on a MacBook laptop with CPU of i7-4core 3.5GHz. The compiler is `gcc-7` while the compiling option has been set to `-Ofast` enabling highest optimization level. The MATLAB kernel has been offered by the MATLAB r2018a for Mac. For synthetic experiments, the poses are simulated using

$$\begin{aligned} \tilde{\boldsymbol{A}}_i &= \mathrm{perturb}\left(\boldsymbol{A}_i, \alpha, \beta\right) \\ \tilde{\boldsymbol{B}}_i &= \mathrm{perturb}\left(\boldsymbol{Y}_{\mathrm{true}}^{-1} \tilde{\boldsymbol{A}}_i \boldsymbol{X}_{\mathrm{true}}, \alpha, \beta\right) \end{aligned} \tag{22}$$

in which $\mathrm{perturb}$ denotes an operator for adding noise perturbation to the true measurements from true poses $\boldsymbol{X}_{\mathrm{true}}$ and $\boldsymbol{Y}_{\mathrm{true}}$, in which α and β denote the noise levels of rotational and translation parts respectively. The perturbation models are

$$\boldsymbol{R}_{\tilde{\boldsymbol{A}}_i} = \boldsymbol{R}_{\boldsymbol{A}_i} \exp(\boldsymbol{\xi}_\times), \qquad \boldsymbol{\xi} \sim \mathcal{N}\left(\boldsymbol{0}, \alpha \boldsymbol{I}\right) \tag{23}$$

$$\boldsymbol{t}_{\tilde{\boldsymbol{A}}_i} = \boldsymbol{t}_{\boldsymbol{A}_i} + \boldsymbol{\eta}, \qquad \boldsymbol{\eta} \sim \mathcal{N}\left(\boldsymbol{0}, \beta \boldsymbol{I}\right) \tag{24}$$

which is the same with models of other poses. In this way, both $\tilde{\boldsymbol{A}}_i$ and $\tilde{\boldsymbol{B}}_i$ are perturbed measurements for HEC computation. Note that if the problem is $\boldsymbol{AX} = \boldsymbol{XB}$, the above models can be adjusted by letting $\boldsymbol{X} = \boldsymbol{Y}$. During simulation, the true values of $\boldsymbol{A}_i$ and $\boldsymbol{B}_i$ are generated making sure that the translational parts are almost normalized so that α and β can well reflect the signal-noise ratio (SNR). The rotation error of a computed pose $\boldsymbol{X}$ with respect to its truth $\boldsymbol{X}_{\mathrm{true}}$ is defined by

$$\boldsymbol{\theta}_{\boldsymbol{X},\mathrm{err}} = \left[\log\left(\boldsymbol{R}_{\boldsymbol{X}} \boldsymbol{R}_{\boldsymbol{X}_{\mathrm{true}}}\right)\right]^{\wedge} \tag{25}$$

while the translational error is

$$\boldsymbol{t}_{\boldsymbol{X},\mathrm{err}} = \boldsymbol{t}_{\boldsymbol{X}} - \boldsymbol{t}_{\boldsymbol{X}_{\mathrm{true}}}. \tag{26}$$

These error indices are some times evaluated via $\left\|\boldsymbol{\theta}_{\boldsymbol{X},\mathrm{err}}\right\| / \sqrt{3}$ and $\left\|\boldsymbol{t}_{\boldsymbol{X},\mathrm{err}}\right\| / \sqrt{3}$ to illustrate the mean error for each axis.

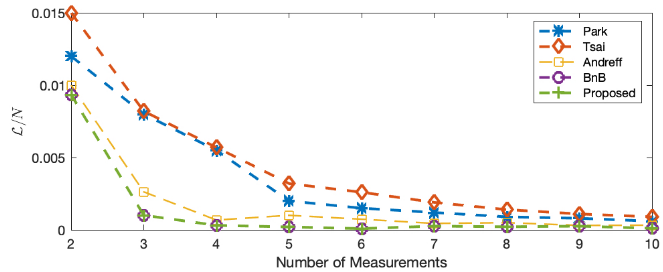

Fig. 2. Loss function values in terms increasing number of measurements.

A. Synthetic Experiment: Common Case

Using the simulation model (22), it is able for us to study the noise characteristics and computational efficiency of multiple methods. We simulate 9 cases where the numbers of measurement pairs ranging from 2 to 10. Each cases are randomly simulated using different combinations of noise levels α and β. Each experiment has been repeated for 1000 times to generate averaged results. Given a certain set of $\alpha = 1 \times 10^{-2}$ and $\beta = 1 \times 10^{-2}$, the accuracy sensitivities of $\boldsymbol{AX} = \boldsymbol{XB}$ solvers in terms of the number of measurements are summarized in Fig. 2, in which we compare the proposed method with other representatives. For $\boldsymbol{AX} = \boldsymbol{XB}$, we use methods of Park et al. [11], Tsai et al. [6], Andreff et al. [13] and BnB method by Heller et al. [16]. To study the sensitivities of various methods subject to different input noise levels, we conduct 1000 random simulations for mean performance. The methods of Park et al., Tsai et al. and Andreff et al. are all analytical but Andreff's method solves the $\boldsymbol{AX} = \boldsymbol{XB}$ problem in a simultaneous manner for rotation and translation. From Fig. 3 and Fig. 4, we are able to see that Andreff's method outperforms the other two analytical approaches. With increasing noise level, the errors of all candidates raise accordingly. The BnB method is a globally optimal one for $\boldsymbol{AX} = \boldsymbol{XB}$ solving. The proposed method achieves the same accuracy as that of BnB. Thus they are the most accurate ones for problem $\boldsymbol{AX} = \boldsymbol{XB}$.

For $\boldsymbol{AX} = \boldsymbol{YB}$ problem, the algorithms of Shah [27], Zhuang et al. [28], Dornaika et al. [15] and Ha et al. [17] have been compared. Note that for Dornaika's method, we use the iterative one and for the two methods of Dornaika et al. and Ha et al. the gradient-descent step lengths are set identically to $\gamma = 0.1$ for stable convergence. From Fig. 5 and Fig. 6, the noise sensitivity of pose errors will be depicted. In these comparisons, the noise level has been visualized in a mixed manner simply because here $\boldsymbol{X}$ and $\boldsymbol{Y}$ is coupled together. One may observe that the error scale also goes up with

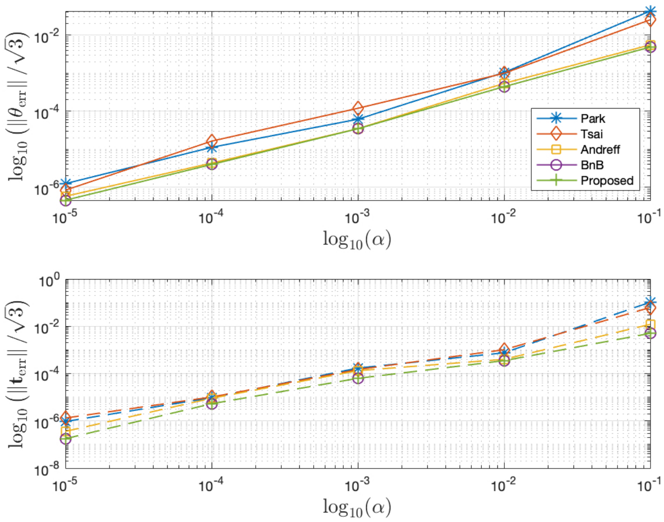

Fig. 3. Sensitivity of $\boldsymbol{AX} = \boldsymbol{XB}$ pose errors to different rotational noise levels $\boldsymbol{\alpha}$.

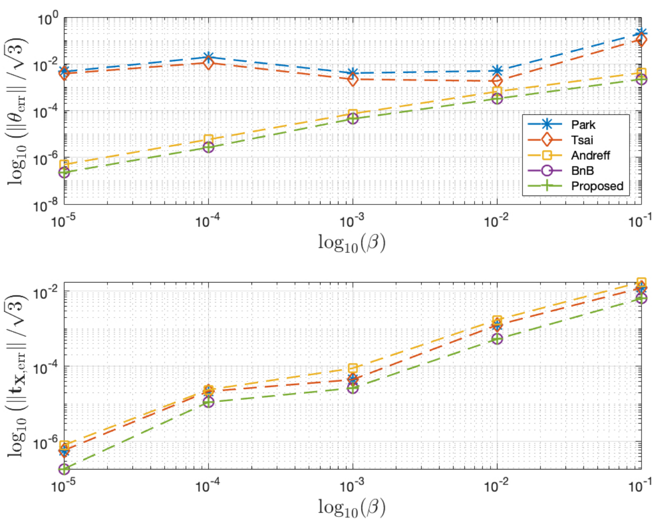

Fig. 4. Sensitivity of $\boldsymbol{AX} = \boldsymbol{XB}$ pose errors to different translational noise levels $\boldsymbol{\beta}$.

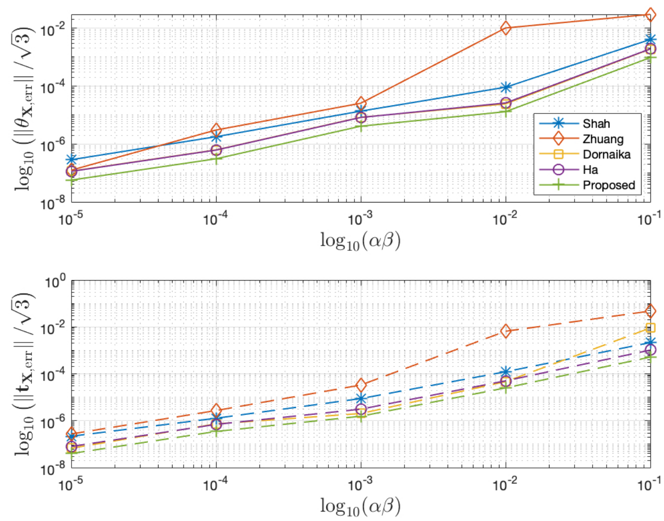

Fig. 5. Sensitivity of pose errors of $\boldsymbol{X}$ in $\boldsymbol{AX} = \boldsymbol{YB}$ to different mixed noise levels $\boldsymbol{\alpha\beta}$.

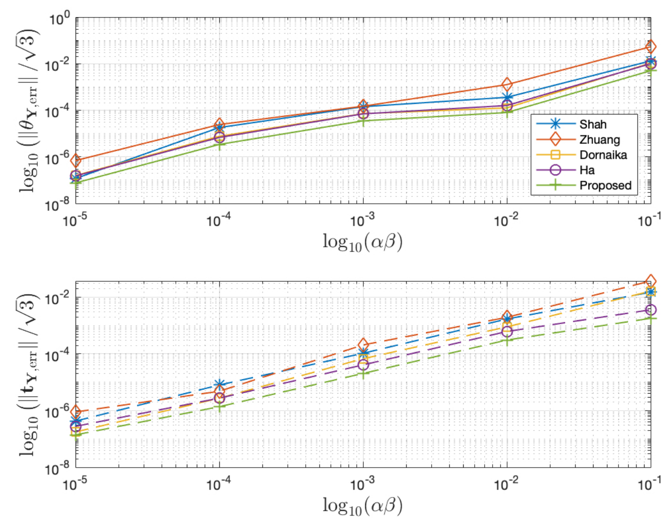

Fig. 6. Sensitivity of pose errors of $\boldsymbol{Y}$ in $\boldsymbol{AX} = \boldsymbol{YB}$ to different mixed noise levels $\boldsymbol{\alpha\beta}$.

increasing mixed noise levels. The methods of Shah, Zhuang et al are analytical ones which can not achieve good accuracy with large noise levels. While the algorithm of Dornaika et al. performs better, it is not likely to be more accurate than the method of Ha et al., which was designed as a global optimizer. However, since there are infinite uniform samplings on $SO(3)$, it is hard to guarantee that the method of Ha et al. will always reach the global optimum. Besides, gradient-based optimizers often suffer from uncertain step lengths. Using a set of synthetic data, we are able to perform two convergence plots, as presented in Fig. 7 and Fig. 8. For each simulation, 200 trials are performed to search global optimum and each trial has the maximum iteration of 500.

We can see that according to different values of γ, the gradient optimizer of Ha et al. can not always find the global optimum. Rather, for $\gamma = 0.01$, all the trials are trivial. In engineering, for different cases, it is hard for us to give a certain γ that is universal for all kinds of datasets. The proposed method, however, is free of online gradient evaluation and will not be subjected to uncertain step lengths. Thus, in summary, the proposed method achieves all local minima and finally obtains the global optimum by sorting all loss function values. From theoretical results shown previously in this paper, it is concluded that the total amount of local minima can reach up to 1080. That is to say for a complete classification of all roots, gradient searching will be at least performed for 1080 times for global optimum, which brings about large computational burden in engineering.

B. Synthetic Experiment: Singular Case

For most HEC tasks, the data will be reasonable for computation. However, in some online calibration works, it is hard to select optimal motion sequences. The example presented in this sub-section shows that some local minima are quite close to each other, making the optimization searching very tough in engineering. A typical case is the pure translational

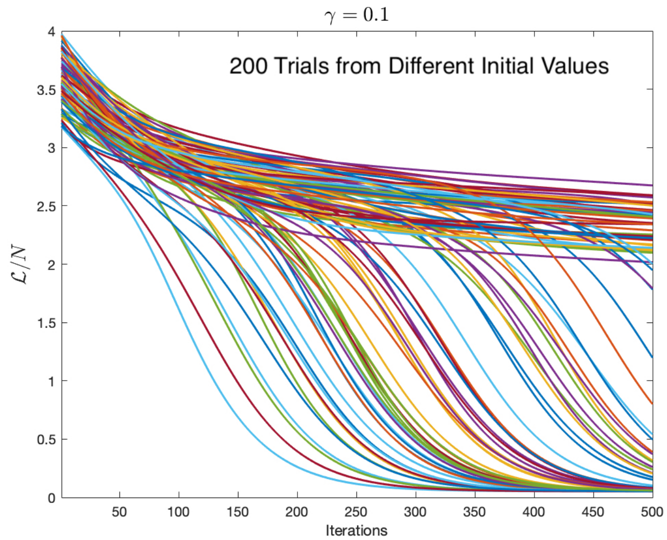

Fig. 7. Typical convergence of the loss function value when the step length of method of Ha et al. [17] is $\gamma = \mathbf{0.1}$ of 200 trials.

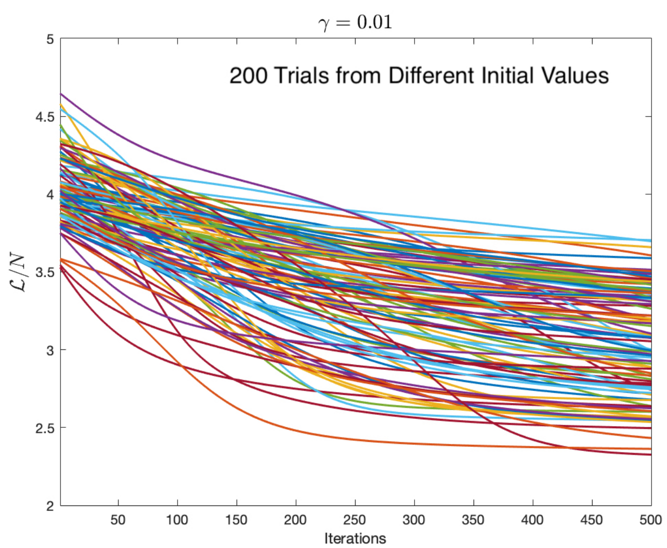

Fig. 8. Typical convergence of the loss function value when the step length of method of Ha et al. [17] is $\gamma = \mathbf{0.01}$ of 200 trials.

motion. For instance, a simulative case is shown in Fig. 9. In such a case, the rotational motion is neglectable, leading to unobservability of translational parts. To illustrate such example, we generate a synthetic dataset with only two pose pairs for HEC problem $\boldsymbol{AX} = \boldsymbol{XB}$. The ground truth is

$$\boldsymbol{X}_{\mathrm{true}} = \begin{pmatrix} 0.24107 & 0.96967 & -0.04024 & 0.30248 \\ -0.28382 & 0.11009 & 0.95254 & 0.67896 \\ 0.92808 & -0.21821 & 0.30175 & 0.67485 \\ 0 & 0 & 0 & 1 \end{pmatrix}. \tag{27}$$

The measurements are

$$\boldsymbol{A}_1 = \begin{pmatrix} 1 & \varrho_{11} & \varrho_{12} & -1.16410 \\ -\varrho_{11} & 1 & \varrho_{13} & -0.43029 \\ -\varrho_{12} & -\varrho_{13} & 1 & -0.45538 \\ 0 & 0 & 0 & 1 \end{pmatrix} \tag{28}$$

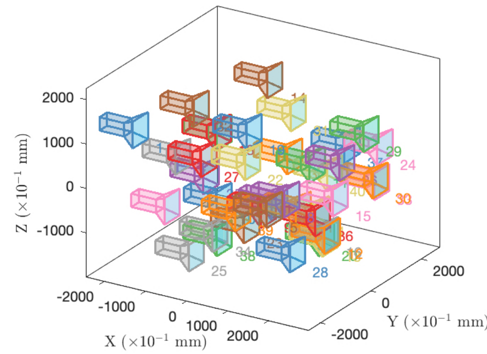

Fig. 9. A pure-translation case.

$$\boldsymbol{A}_2 = \begin{pmatrix} 1 & \varrho_{21} & \varrho_{22} & 0.31605 \\ -\varrho_{21} & 1 & \varrho_{23} & 0.73459 \\ -\varrho_{22} & -\varrho_{23} & 1 & 0.88189 \\ 0 & 0 & 0 & 1 \end{pmatrix} \tag{29}$$

$$\boldsymbol{B}_1 = \begin{pmatrix} 1 & \varrho_{31} & \varrho_{32} & -0.58113 \\ -\varrho_{31} & 1 & \varrho_{33} & -1.07680 \\ -\varrho_{32} & -\varrho_{33} & 1 & -0.50043 \\ 0 & 0 & 0 & 1 \end{pmatrix} \tag{30}$$

$$\boldsymbol{B}_2 = \begin{pmatrix} 1 & \varrho_{41} & \varrho_{42} & 0.68616 \\ -\varrho_{41} & 1 & \varrho_{43} & 0.19490 \\ -\varrho_{42} & -\varrho_{43} & 1 & 0.95311 \\ 0 & 0 & 0 & 1 \end{pmatrix} \tag{31}$$

(32)

in which the parameters are

$$\varrho_{11} = 1.39189247687321 \times 10^{-12} \tag{33}$$
$$\varrho_{12} = 1.30861934823665 \times 10^{-12} \tag{34}$$
$$\varrho_{13} = 1.69398839073174 \times 10^{-13} \tag{35}$$
$$\varrho_{21} = 3.33074698336478 \times 10^{-13} \tag{36}$$
$$\varrho_{22} = -4.74495911429954 \times 10^{-13} \tag{37}$$
$$\varrho_{23} = -8.21458870144532 \times 10^{-13} \tag{38}$$
$$\varrho_{31} = -1.09043432460593 \times 10^{-12} \tag{39}$$
$$\varrho_{32} = 4.00144747045421 \times 10^{-13} \tag{40}$$
$$\varrho_{33} = 2.64665852962922 \times 10^{-12} \tag{41}$$
$$\varrho_{41} = -4.26681754439078 \times 10^{-13} \tag{42}$$
$$\varrho_{42} = -4.78662744237887 \times 10^{-13} \tag{43}$$
$$\varrho_{43} = -1.6696207320982 \times 10^{-12}. \tag{44}$$

Using the developed algorithm, it is able for us to compute all the local minima, of which the least several loss function values among total 243 ones in ascending order are

$$\begin{aligned} \mathcal{L} &= 2.18140848054451 \times 10^{-22} \\ \mathcal{L} &= 2.09547579288484 \times 10^{-9} \\ \mathcal{L} &= 3.72529029846192 \times 10^{-8} \\ \mathcal{L} &= 5.96046447753907 \times 10^{-8} \\ \mathcal{L} &= 0.0170645634643734 \\ \mathcal{L} &= 0.0174178176093847 \\ \mathcal{L} &= 0.0261864693893585 \\ \mathcal{L} &= 0.0267650652676821 \\ \mathcal{L} &= 0.028603101382032 \\ \mathcal{L} &= 0.0294563099741936 \\ \mathcal{L} &= 0.521159673109651. \end{aligned} \tag{45}$$

Note that the above rotational parts are generated using the small-angle approximation (infinitesimal) of rotation matrix (See Eq. 6 in [29] and Eq. 25 in [30]). From these values, one may see that the differences between successive loss function values are small. This will lead to quite tough searching by using gradient optimizers. And eventually, the method of Ha et al. fails for this case even if the step length γ has been tuned for multiple times. This extreme case shows that previous methods are not always able to locate all possible local minima. The proposed method guarantees that all local minima can be found so the global optimality is strictly guaranteed.

Fig. 10. Experimental setup for industrial hand-eye calibration.

C. Real Experiment: Industrial Hand-Eye Calibration

An industrial robotic manipulator UR5 from Universal Robot is employed for validation (see Fig. 10). A 12×9 standard chessboard with each block of 30mm width has been used as the origin plane of the world frame. An Intel Realsense D435i camera has been attached to the flange of the robotic manipulator where another industrial gripper is installed for visually aided grasping. We use the algorithm in [31] to detect the corners of chessboard. The command `perf` is invoked for run-time stats and the parallelization has been enabled by the compiler option `-Ofast`. The hand-eye problem now turns into finding out the unknown transform $\boldsymbol{X}$ between the flange frame and the Realsense camera. This can be achieved independently by using solvers of $\boldsymbol{AX} = \boldsymbol{XB}$ and $\boldsymbol{AX} = \boldsymbol{YB}$ problems. The calibration accuracy can be estimated by mapping the pose back into the 2D imaging plane, which produces the reprojection errors between detected corners of the checkerboard. We generate different poses of manipulators to acquired perspective imaging of the chessboard. The reprojection errors using $\boldsymbol{AX} = \boldsymbol{XB}$ for one of the generated datasets are shown in Fig. 11.

The results indicate that the proposed symbolic method is accurate, with mean reprojection errors of 0.12 pixels in vertical direction and 0.11 pixels in horizontal direction. We would also like to study the computational efficiency of various algorithms. Using different numbers of poses, all candidates compared in previously are chosen for computational

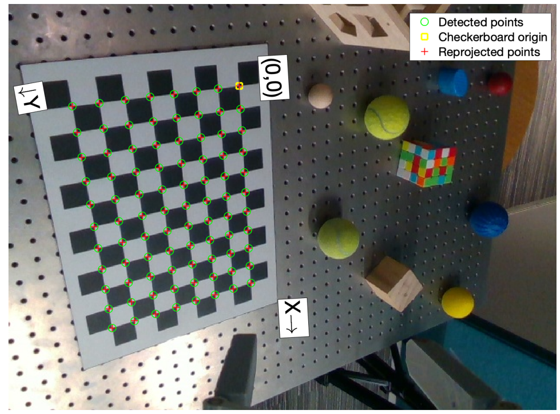

Fig. 11. The reprojection errors of the $\boldsymbol{AX} = \boldsymbol{XB}$ calibration.

evaluation. The main computational stats on the employed laptop are summarized in Table I and Table II in which the mean performances have been visualized. We can see that the global iterative methods like BnB and method of Ha et al. are quite time-consuming for large datasets. This is because these algorithms will either require extensive matching or conduct huge loads of loss-function evaluation. Analytical methods are computationally efficient but they can not achieve global optimum and sometimes may fail in the presence of datasets with outliers. The proposed method, however, does not need computation of gradient over and over again. Instead, it directly solves the polynomial system algebraically. Thus the computational performance for large datasets will be much more satisfactory than other globally optimal representatives. Further applications are not limited to industrial hand-eye calibration but may also include camera/camera, camera/laser, camera/inertial calibration as well.

IV. Conclusion

Two classical HEC problems $\boldsymbol{AX} = \boldsymbol{XB}$ and $\boldsymbol{AX} = \boldsymbol{YB}$ have been revisited in this paper. A new error formulation using Caylay transform has been proposed for the first time. This new formulation allows for a unified approach for $\boldsymbol{AX} = \boldsymbol{XB}$ and $\boldsymbol{AX} = \boldsymbol{YB}$ simultaneously. Using the generated optimization target, algebraic polynomial system has been derived. The new aim has been shifted to algebraically solve this system for all possible roots. Wu's elimination method has been invoked to achieve this goal and the accuracy has been proven to be optimal. We reveal the fact the maximum numbers of possible local minima is bounded as 243 for $\boldsymbol{AX} = \boldsymbol{XB}$ and 1080 for $\boldsymbol{AX} = \boldsymbol{YB}$. It is investigated that the proposed method is also robust for some extreme cases while some representatives can not give global optimum. Industrial hand-eye calibration tasks also validate the accuracy and better computational performance compared with recent representatives.

However, we could see that the numbers of possible local minima are large, leading to sophisticated symbolic elimination. Future efforts should be devoted to find a better framework to significantly reduce such symbolic manipulations. Improvements may be conducted via advanced symbolic reduction techniques regarding the specific hand-eye problem.

TABLE I
COMPUTATIONAL PERFORMANCES OF VARIOUS ALGORITHMS FOR $\boldsymbol{AX}=\boldsymbol{XB}$ PROBLEM (SEC)

Measurement Number N	Park	Tsai	Andreff	Branch-and-Bound	Proposed ($\boldsymbol{AX}=\boldsymbol{XB}$)
5	3.7×10^{-3}	6.4×10^{-3}	7.4×10^{-4}	5.5×10^{-1}	7.2×10^{-1}
100	8.9×10^{-3}	3.3×10^{-2}	2.7×10^{-3}	6.1	8.3×10^{-2}
1000	4.6×10^{-2}	9.2×10^{-2}	8.3×10^{-3}	82	1.1
10000	9.3×10^{-2}	3.2×10^{-1}	2.6×10^{-2}	907	2.4
100000	4.4×10^{-1}	1.6	9.1×10^{-1}	14321	4.6

TABLE II
COMPUTATIONAL PERFORMANCES OF VARIOUS ALGORITHMS FOR $\boldsymbol{AX}=\boldsymbol{YB}$ PROBLEM (SEC)

Measurement Number N	Shah	Zhuang	Dornaika	Ha	Proposed ($\boldsymbol{AX}=\boldsymbol{YB}$)
5	1.4×10^{-3}	8.2×10^{-3}	7.6×10^{-2}	9.7×10^{-2}	3.8
100	3.2×10^{-2}	5.1×10^{-2}	6.3×10^{-1}	6.1	4.6
1000	4.3×10^{-2}	9.7×10^{-2}	3.5	9.3	6.2
10000	8.7×10^{-2}	7.2×10^{-1}	32	206	8.3
100000	3.9×10^{-1}	4.5	301	3783	10.1

ACKNOWLEDGMENT

The experimental study was carried out during COVID-19 pandemic in Tencent Robotics X, Shenzhen, China. We would like to thank Dr. Yu Zheng from Tencent Robotics X for constructive discussions.

REFERENCES

[1] A. Muis and K. Ohnishi, "Eye-to-hand approach on eye-in-hand configuration within real-time visual servoing," *IEEE/ASME Trans. Mechatronics*, vol. 10, no. 4, pp. 404–410, 2005.
[2] J. S. Hu and Y. J. Chang, "Automatic calibration of hand-eye-workspace and camera using hand-mounted line laser," *IEEE/ASME Trans. Mechatronics*, vol. 18, no. 6, pp. 1778–1786, 2013.
[3] Y. C. Shiu and S. Ahmad, "Calibration of Wrist-Mounted Robotic Sensors by Solving Homogeneous Transform Equations of the Form AX = XB," *IEEE Trans. Robot. Autom.*, vol. 5, no. 1, pp. 16–29, 1989.
[4] D. Modenini, "Attitude determination from ellipsoid observations: A modified orthogonal procrustes problem," *AIAA J. Guid. Control Dyn.*, vol. 41, no. 10, pp. 2320–2325, 2018.
[5] J. Wu, "Unified Attitude Determination Problem from Vector Observations and Hand-eye Measurements," *IEEE Trans. Aerosp. Elect. Syst.*, vol. 00, no. 00, pp. 1–1, 2020.
[6] R. Y. Tsai and R. K. Lenz, "A New Technique for Fully Autonomous and Efficient 3D Robotics Hand/Eye Calibration," *IEEE Trans. Robot. Autom.*, vol. 5, no. 3, pp. 345–358, 1989.
[7] J. C. Chou and M. Kamel, "Finding the position and orientation of a sensor on a robot manipulator using quaternions," *Int. J. Rob. Res.*, vol. 10, no. 3, pp. 240–254, 1991.
[8] K. Daniilidis, "Hand-Eye Calibration Using Dual Quaternions," *Int. J. Rob. Res.*, vol. 18, no. 3, pp. 286–298, 1999.
[9] Z. Zhao and Y. Liu, "A hand-eye calibration algorithm based on screw motions," *Robotica*, vol. 27, no. 2, pp. 217–223, 2009.
[10] J. Wu, Y. Sun, M. Wang, and M. Liu, "Hand-eye Calibration: 4D Procrustes Analysis Approach," *IEEE Trans. Instrum. Meas.*, pp. 1–1, 2019.
[11] F. C. Park and B. J. Martin, "Robot Sensor Calibration: Solving AX = XB on the Euclidean Group," *IEEE Trans. Robot. Autom.*, vol. 10, no. 5, pp. 717–721, 1994.
[12] S. Qiu, M. Wang, and M. R. Kermani, "A New Formulation for Hand-Eye Calibrations as Point Set Matching," *IEEE Trans. Instrum. Meas.*, vol. 9456, no. 2, pp. 1–1, 2020.
[13] N. Andreff, R. Horaud, and B. Espiau, "Robot Hand-Eye Calibration Using Structure-from-Motion," *Int. J. Rob. Res.*, vol. 20, no. 3, pp. 228–248, 2001.
[14] R. Horaud and F. Dornaika, "Hand-Eye Calibration," *Int. J. Rob. Res.*, vol. 14, no. 3, pp. 195–210, 1995.
[15] F. Dornaika and R. Horaud, "Simultaneous Robot-World and Hand-Eye Calibration," *IEEE Trans. Robot. Autom.*, vol. 14, no. 4, pp. 617–622, 1998.
[16] J. Heller, M. Havlena, and T. Pajdla, "Globally Optimal Hand-Eye Calibration Using Branch-and-Bound," *IEEE Trans. Pattern Anal. Mach. Intell.*, vol. 38, no. 5, pp. 1027–1033, 2016.
[17] J. Ha, D. Kang, and F. C. Park, "A Stochastic Global Optimization Algorithm for the Two-Frame Sensor Calibration Problem," *IEEE Trans. Ind. Electron.*, vol. 63, no. 4, pp. 2434–2446, 2016.
[18] J. Yang, H. Li, D. Campbell, and Y. Jia, "Go-ICP: A Globally Optimal Solution to 3D ICP Point-Set Registration," *IEEE Trans. Pattern Anal. Mach. Intell.*, vol. 38, no. 11, pp. 2241–2254, 2016.
[19] A. Parra Bustos, T. J. Chin, A. Eriksson, H. Li, and D. Suter, "Fast Rotation Search with Stereographic Projections for 3D Registration," *IEEE Trans. Pattern Anal. Mach. Intell.*, vol. 38, no. 11, pp. 2227–2240, 2016.
[20] H. Bettahar, O. Lehmann, C. Clevy, N. Courjal, and P. Lutz, "Photo-robotic Extrinsic Parameters calibration of 6-DOF Robot for High Positioning Accuracy," *IEEE/ASME Trans. Mechatronics*, vol. 25, no. 2, pp. 1–1, 2020.
[21] Z. Q. Zhang, "Cameras and Inertial/Magnetic Sensor Units Alignment Calibration," *IEEE Trans. Instrum. Meas.*, vol. 65, no. 6, pp. 1495–1502, 2016.
[22] J. Rehder, R. Siegwart, and P. Furgale, "A General Approach to Spatiotemporal Calibration in Multisensor Systems," *IEEE Trans. Robot.*, vol. 32, no. 2, pp. 383–398, 2016.
[23] J. Heller, D. Henrion, and T. Pajdla, "Hand-eye and robot-world calibration by global polynomial optimization," *Proc. - IEEE Int. Conf. Robot. Autom.*, pp. 3157–3164, 2014.
[24] W. Wen-Tsun, *Selected Works of Wen-Tsun Wu*. World Scientific, 2008.
[25] ——, "Basic principles of mechanical theorem proving in elementary geometries," *J. Automat. Reason.*, vol. 2, no. 3, pp. 221–252, 1986.
[26] R. L. Rivest, A. Shamir, and L. Adleman, "A method for obtaining digital signatures and public-key cryptosystems," *Commun. ACM*, vol. 21, no. 2, pp. 120–126, 1978.
[27] M. Shah, "Solving the Robot-World/Hand-Eye Calibration Problem Using the Kronecker Product," *J. Mech. Robot.*, vol. 5, no. 3, p. 031007, 2013.
[28] H. Zhuang, Z. S. Roth, and R. Sudhakar, "Simultaneous robot/world and tool/flange calibration by solving homogeneous transformation equations of the form AX = YB," *IEEE Trans. Robot. Autom.*, vol. 10, no. 4, pp. 549–554, 1994.
[29] A. Nüchter, J. Elseberg, P. Schneider, and D. Paulus, "Linearization of rotations for globally consistent n-scan matching," *IEEE ICRA*, pp. 1373–1379, 2010.
[30] T. Barfoot, J. R. Forbes, and P. T. Furgale, "Pose estimation using linearized rotations and quaternion algebra," *Acta Astronaut.*, vol. 68, no. 1-2, pp. 101–112, 2011.
[31] A. Geiger, F. Moosmann, Ö. Car, and B. Schuster, "Automatic camera and range sensor calibration using a single shot," *IEEE ICRA*, pp. 3936–3943, 2012.

Jin Wu (S'15-M'17) was born in May, 1994 in Zhenjiang, Jiangsu, China. He received the B.S. Degree from University of Electronic Science and Technology of China, Chengdu, China. He has been a research assistant (PhD student) in Department of Electronic and Computer Engineering, Hong Kong University of Science and Technology (HKUST). His research interests include robot navigation, multi-sensor fusion, automatic control and mechatronics. One of his papers published in IEEE TRANSACTIONS ON AUTOMATION SCIENCE AND ENGINEERING was selected as the ESI Highly Cited Paper by ISI Web of Science in 2018.

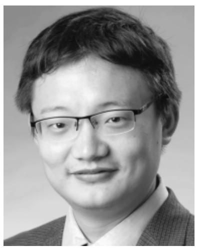

Ming Liu (S'12-M'13-SM'18) received the B.A. degree in automation from Tongji University, Shanghai, China, in 2005, and the Ph.D. degree from the Department of Mechanical and Process Engineering, ETH Zürich, Zürich, Switzerland, in 2013, supervised by Prof. Roland Siegwart.

He is currently with the Department of Electronic and Computer Engineering, Hong Kong University of Science and Technology (HKUST), Hong Kong, as an Associate Professor. He is coordinating and involved in NSF Projects and National 863-Hi-TechPlan Projects in China. His research interests include dynamic environment modeling, deep-learning for robotics, 3-D mapping, and visual control. Dr. Liu was a recipient of the Best Paper Award in Information for IEEE ICIA 2013 as first author, the Best Paper Award Finalists as co-author, the Best RoboCup Paper Award for IEEE IROS 2013, the Best Conference Paper Award for IEEE-CYBER 2015, the Best Student Paper Finalist for IEEE RCAR 2015, the Best Student Paper Finalist for IEEE ROBIO 2015, the Best Student Paper Award for IEEE ICAR 2017, the Best Paper in Automation Award for IEEE ICIA 2017, twice the innovation contest Chunhui Cup Winning Award in 2012 and 2013, and the Wu Wenjun AI Award in 2016. Dr. Liu is currently an Associate Editor for IEEE ROBOTICS AND AUTOMATION LETTERS, *IET Cyber-Systems and Robotics*, *International Journal of Robotics and Automation*. He is a Senior Member of IEEE.

Yilong Zhu was born in 1994. He received B.Sc. in measurement and control technology and instruments from Harbin Institute of Technology, China, in 2017, and the M.S degree in electrical engineering from Hong Kong University of Science and Technology, Hong Kong, China, in 2018. He is currently working toward the Ph.D degree in the robotics and multi-perception laboratory (RAM-LAB) with Hong Kong University of Science and Technology, Hong Kong, China, where his research mainly focuses on LiDAR and sensor fusion for robotics. He won the Best Paper Finalist Award in 2019 IEEE International Conference on Robotics and Biomimetics (ROBIO). His research interests include SLAM, sensor fusion and robotic perception.

Zuhao Zou was born in 1994. He received B.Sc. degree from University of Newcastle, in 2016, and the M.S degree in electrical engineering from University of London College in 2018, under the supervision of Prof. Simon Julier. He is currently a navigation algorithm engineer in Unity Drive Inc., Shenzhen, China. His research interests include inertial navigation, mechatronics and robotics, localization and mapping.

Ming-Zhe Dai received the B.S. and M.S. degrees in detection, guidance, and control technology and optical engineering from Harbin Engineering University, China, in 2011 and 2014, Ph.D. degree in control science and engineering from Harbin Institute of Technology, China, in 2019.

Now he is a lecturer at Central South University. His current research interests include coordination of multi-agent systems, event-triggered control, and spacecraft control.

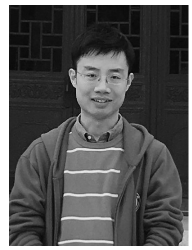

Chengxi Zhang (M'20) was born in Feb, 1990, Shandong, China. He received his B.S. and M.S. degrees in microelectronics and solid-state electronics at Harbin Institute of Technology, China, in 2012 and 2015. He received his Ph.D. degree in control science and engineering at Shanghai Jiao Tong University, China, in 2019. He is a board member of the Shanghai Jiao Tong University Ph.D. Alumni Association of the School of Aeronautics and Astronautics, from 2019 to 2024.

Currently, he is a Post-doctoral fellow at School of Electronic and Information Engineering, Harbin Institute of Technology, Shenzhen campus, China. His research interests are embedded system software and hardware design, information fusion and control theory.

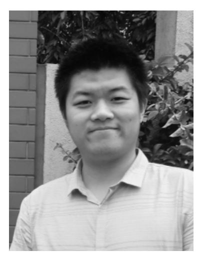

Yi Jiang (S'14-M'20) was born in Ezhou, Hubei, China. He received the B. Eng. degree in automation, M.S. and Ph.D. degrees in control theory and control engineering from Information Science and Engineering College and State Key Laboratory of Synthetical Automation for Process Industries in Northeastern University, Shenyang, Liaoning, China in 2014, 2016 and 2020, respectively.

From January to July, 2017, he was a Visiting Scholar with the UTA Research Institute, University of Texas at Arlington, TX, USA, and from March 2018 to March 2019, he was a Research Assistant with the University of Alberta, Edmonton, Canada. His research interests include networked control systems, industrial process operational control, reinforcement learning and event-triggered control.

Dr. Jiang is an Associate Editor for *Advanced Control for Applications: Engineering and Industrial Systems*.

Chong Li (S'15-M'17) received his B.S. and M.S. in Automation and Control Theory & Engineering, from Ocean University of China, Qingdao, China, in 2009 and 2012, respectively. He received his Ph.D in Mechanical Engineering, from Auburn University, Auburn, AL, United States, in 2016. Then he joined iMEMS Lab at Georgia Tech as a postdoctoral research fellow from 2016 to 2018.

Currently, Dr. Chong Li is an Associate Professor with Department of Automation & Measurement, Ocean University of China. His research interests include precision control systems, resonant gyroscopes, navigation & guidance, and instrumentation technology.